BIOLOGICAL SCIENCES: Medical Sciences

# Proteolytic cleavage of Ser52Pro variant transthyretin triggers its amyloid fibrillogenesis

Short title: Transthyretin proteolysis and fibrillogenesis

**P. Patrizia Mangione[a,b], Riccardo Porcari[a], Julian D. Gillmore[a], Piero Pucci[c], Maria Monti[c], Mattia Porcari[b], Sofia Giorgetti[b], Loredana Marchese[b], Sara Raimondi[b], Louise C. Serpell[d], Wenjie Chen[e], Annalisa Relini[f], Julien Marcoux[g], Innes R. Clatworthy[h], Graham W. Taylor[a], Glenys A. Tennent[a], Carol V. Robinson[g], Philip N. Hawkins[a], Monica Stoppini[b], Stephen P. Wood[a,e], Mark B. Pepys[a], and Vittorio Bellotti[a,b,1]**

[a]Wolfson Drug Discovery Unit, Centre for Amyloidosis and Acute Phase Proteins, Division of Medicine, University College London, London NW3 2PF, UK; [b]Department of Molecular Medicine, Institute of Biochemistry, University of Pavia, 27100 Pavia, Italy; [c]Department of Chemical Sciences and CEINGE Advanced Biotechnologies, University of Naples Federico II, 80145 Naples, Italy; [d]School of Life Sciences, University of Sussex, Falmer BN1 9QG, UK; [e]Laboratory of Protein Crystallography, Centre for Amyloidosis and Acute Phase Proteins, University College London, London NW3 2PF, UK; [f]Department of Physics, University of Genoa, 16146 Genoa, Italy; [g]Department of Chemistry, University of Oxford, Oxford OX1 3TA, UK and [h]Electron Microscopy Unit, University College London, London NW3 2PF, UK.

[1]To whom correspondence should be addressed. Wolfson Drug Discovery Unit, Centre for Amyloidosis and Acute Phase Proteins, Division of Medicine, University College London, Rowland Hill Street, London NW3 2PF, UK. Tel: +44 20 7433 2773; Fax: +44 20 7433 2803; E-mail: v.bellotti@ucl.ac.uk.

Keywords: amyloid, transthyretin, fibrillogenesis, proteolysis

**The Ser52Pro variant of transthyretin (TTR) produces aggressive, highly penetrant, autosomal dominant systemic amyloidosis in patients heterozygous for the causative mutation. Together with a minor quantity of full length wild type and variant TTR, the main component of the ex vivo fibrils was the residue 49-127 fragment of the TTR variant, the same portion of the TTR sequence which has previously been reported as the principal constituent of type A, cardiac amyloid fibrils formed from wild type TTR and other TTR variants [Bergstrom J, et al. (2005) *J Pathol* 206(2):224–232]. This specific truncation of Ser52Pro TTR was readily generated in vitro by limited proteolysis. In physiological conditions and under agitation the residue 49-127 proteolytic fragment rapidly and completely self-aggregates into typical amyloid fibrils. The remarkable susceptibility to such cleavage is likely due to localized destabilization of the β-turn linking strands C and D caused by loss of the wild type hydrogen bonding network between the side chains of residues Ser52, Glu54, Ser50 and a water molecule, as revealed by the high resolution crystallographic structure of Ser52Pro TTR. We thus provide a structural basis for the recently hypothesized, crucial pathogenic role of proteolytic cleavage in TTR amyloid fibrillogenesis. Binding by Ser52Pro variant TTR of the natural ligands, thyroxine or retinol binding protein (RBP), stabilizes the native tetrameric assembly, but neither protected the variant from proteolysis. Interestingly, however, binding of RBP but not thyroxine inhibited subsequent fibrillogenesis.**

## Significance

Transthyretin, a normal circulating plasma protein, is inherently amyloidogenic. It forms abnormal, insoluble, extracellular amyloid fibrils in the elderly, sometimes causing structural and functional damage leading to disease, senile amyloidosis. Over 100 different point mutations in the transthyretin gene cause earlier adult onset, autosomal dominant, fatal, hereditary amyloidosis. Ser52Pro variant transthyretin is responsible for the most aggressive known clinical phenotype. Here we identify the crucial pathogenic role of specific proteolytic cleavage at residue 48 in triggering fibril formation by this variant. Genuine amyloid fibril formation *in vitro* is much more extensive than previously reported for wild type or any other transthyretin variant. Characterization of the fibrillogenic effect of this cleavage powerfully informs drug design and targeting for transthyretin amyloidosis.

Amyloidosis is caused by extracellular accumulation of abnormal protein fibrils in various tissues throughout the body (1). Hereditary systemic amyloidosis is a variably penetrant autosomal dominant condition caused by mutations encoding usually single residue substitutions in certain globular proteins, including transthyretin, apolipoprotein-AI, fibrinogen A α-chain (2), gelsolin, lysozyme, cystatin C and $\beta_2$-microglobulin (3). Individuals heterozygous for the causative mutated genes produce variant proteins that are less stable than their wild type counterparts and consequently have a propensity to misfold and then aggregate in the characteristic amyloid fibril conformation and deposit in the tissues. Transthyretin (TTR) variants, encoded by more than 100 different amyloidogenic mutations (http://amyloidosismutations.com/attr.html), are by far the most common cause of hereditary amyloidosis, although there are only ~10,000 cases worldwide.

Elucidation of the mechanism of amyloidogenic conversion of TTR has been challenging and has not hitherto been revealed by any obvious feature of the native protein structure despite very high resolution crystallography of the wild type and several amyloidogenic variants (4). The native tetrameric assemblies of all amyloidogenic TTR variants studied so far are less stable in vitro than wild type TTR, while the Thr119Met variant is more stable and is known to protect carriers of amyloidogenic mutations from developing TTR amyloidosis (5). It is therefore widely accepted that tetramer dissociation and partial denaturation of released monomers is the crucial and rate limiting pre-requisite for formation of TTR amyloid fibrils (2). However there is no direct supportive evidence of this mechanism in vivo and a key role for post-translational modifications of TTR, including partial proteolysis has been extensively debated (6).

In addition to full length TTR monomers, Lundgren's group identified the residue 49-127 fragment, generated by proteolytic cleavage of the peptide bond Lys48-Thr49 (7), as the main fragment present in ex vivo TTR amyloid fibrils. The protease responsible has not yet been

identified but the highly specific cleavage suggests that it could be a trypsin-like serine protease. Meanwhile Westermark and collaborators have elegantly characterized the constituents of TTR amyloid fibrils extracted from cardiac amyloid deposits and adipose tissue, identifying two clearly distinct categories (8, 9). *Type A* fibrils contain a high proportion of truncated species which are not found in *type B* fibrils composed almost entirely of full length TTR (8). The presence of cleaved fragments is apparently not influenced by the nature or the position of the amino acid substitution (8). Rather it correlates with the abundance of the cardiac amyloid deposits (10), with increased patient age and with late onset disease, being most common in subjects with senile systemic amyloidosis caused by wild type not variant TTR. The possible pathogenic role of proteolytic cleavage is further suggested by the clinical course in patients with hereditary TTR amyloidosis who undergo liver transplantation to replace their variant TTR production with wild type TTR. Individuals with *type A* fibrils in their cardiac deposits have a notably poorer outcome often with rapidly progressive cardiac involvement (11).

Here we report a large kindred in which affected individuals carrying the mutation encoding Ser52Pro variant TTR developed unusually early onset, aggressive and fatal systemic amyloidosis. Rapidly progressive amyloid polyneuropathy, soon followed by symptomatic cardiac amyloidosis, developed in the third decade, typically leading to death within five years. We have now fully characterized the native structure of the variant and the composition of the ex vivo amyloid fibrils, which contain abundant truncated TTR cleaved at the *C*-terminal of residue 48. This specific cleavage was remarkably reproduced by limited proteolysis of the isolated recombinant variant TTR in vitro and we have established that, once released from the native tetrameric protein, the polypeptide 49-127 rapidly self-aggregates into genuine amyloid fibrils.

## Results

**Hereditary Amyloidosis Phenotype**. The proband (Fig. S1*A*, III-2) presented at age 30 with autonomic dysfunction, peripheral neuropathy, euthyroid multinodular goiter and sicca syndrome. A needle biopsy of the thyroid contained extensive TTR amyloid deposits and the causative mutation encoding the Ser52Pro TTR variant was detected by DNA sequencing. $^{123}$I-serum amyloid P component (SAP) scintigraphy (12) demonstrated substantial visceral amyloidosis affecting the spleen, liver, kidneys and adrenal glands. Echocardiography and subsequent cardiac angiography demonstrated an infiltrative restrictive cardiomyopathy with well preserved ventricular function and there were abundant TTR amyloid deposits in an endomyocardial biopsy. He underwent liver transplantation in an attempt to reduce abundance of the amyloidogenic variant but amyloidosis nevertheless progressed rapidly and he died 5 months later with cardiac failure and progressive neuropathy. The proband's mother (II-1) died at age 34 from a progressive neuromuscular disorder and extensive systemic amyloidosis was discovered at post mortem. The clinical picture in subjects II-3 and II-5 was consistent with neuropathic systemic amyloidosis but no histological confirmation was available. The maternal uncle of the propositus (II-3) was diagnosed as paraplegic prior to his death at age 42 in renal failure. Subject II-5 developed thyromegaly from about age 20 and died at age 30 from a neuromuscular disease with a presumptive diagnosis of multiple sclerosis. SAP scintigraphy in the proband's brother (III-3) at age 28 showed extensive amyloid in the spleen, kidneys and adrenal glands, similar to the propositus. He developed amyloid polyneuropathy one year later, and died with progressive amyloidosis, including severe cardiac involvement, 3 months after liver transplantation. The third brother does not carry the TTR mutation and remains

asymptomatic. Two cousins died before age 40 with a similar pattern of disease but including clinically significant leptomeningeal TTR amyloid deposits. One of these subjects underwent liver transplantation when he had only the very earliest symptoms of neuropathy and no definite cardiac amyloid deposition, but died 8 years later having developed profound neuropathy, severe cardiac amyloidosis and dementia. The clinical phenotype in this kindred is among the most severe ever described in ATTR amyloidosis.

**DNA Sequencing.** The proband, his affected brother, and the two affected cousins were heterozygotes for a single point mutation in exon 3 of the TTR gene, encoding substitution of a proline (codon CCT) for serine (codon TCT) at residue 52 of the mature TTR protein (Fig. S1*B*). The father, unaffected brother and unaffected cousins were homozygous for the wild type sequence.

**Amyloid Fibril Protein Typing.** Immunohistochemical staining of the cardiac biopsy from the propositus identified TTR as the amyloid fibril protein (Fig. S1*C*), and the deposits also stained for SAP, the universal non-fibrillar component of all human amyloid.

**Analysis of ex vivo Fibrils.** Ex vivo amyloid fibrils were isolated from the spleen of the propositus removed during liver transplantation and separated by SDS-PAGE (Fig.1*A* and *B*) for further proteomic analysis. The mass mapping analysis of the tryptic peptides from bands 1 and 2 in the gel are shown in Fig. 1*C*. The MALDI-MS spectrum of band 1 showed the presence of several mass signals corresponding to TTR tryptic peptides leading to high protein sequence coverage. In particular, the mass signal at m/z 3150.57 was assigned to the tryptic peptide 49-76 carrying the Ser to Pro amino acid substitution. A small signal at m/z 3140.54 corresponding to

the wild type peptide was also detected. LC-MS/MS analysis of tryptic peptides from band 1 showed that both the wild type and Ser52Pro full length TTR were present with two mass signals at m/z 819.8 and 823.0 corresponding to the triply charged wild type and variant peptides 49-70, respectively. This assignment was confirmed by the MS/MS spectra of the two precursor ions. In contrast, MS analysis of band 2 showed only a single protein species, corresponding to the *C*-terminal fragment of the variant TTR generated by cleavage at residue Lys48. Five cycles of *N*-terminal Edman sequencing of band 2 yielded Thr-Ser-Glu-Pro-Gly, that is residues 49-53 of variant TTR, unequivocally confirming the presence of only proline at position 52 (Fig. S2).

**Authenticity and Stability of Recombinant TTR Proteins.** The subunits of recombinant wild type and Ser52Pro variant TTR proteins had molecular masses of 13892.2 ± 0.9 Da and 13902.1 ± 1.5 respectively, corresponding to the expected theoretical mass values of 13892.6 Da and 13902.7 Da, including the additional *N*-terminal methionine residue, Met 0. Correct assembly of the subunits into native homotetrameric wild type and variant TTR was confirmed by both size exclusion chromatography and native mass spectrometry and these intact proteins bound the natural ligand, thyroxine, normally, showing the same $IC_{50}$ with mds84 and tafamidis (13, 14) as native wild type TTR isolated from normal human serum (Table S1). However the guanidine thiocyanate (Gdn-SCN) mediated transition from folded tetramer to unfolded monomers (5) (Fig. S3) showed that the native tetrameric Ser52Pro variant TTR was significantly destabilized, by 2.3 kcal/mol, compared to the wild type protein, with a midpoint concentration of Gdn-SCN ($C_m$) shifting from mean (SD), $n = 3$, of 1.03 (0.02) M for the wild type to 0.8 (0.06) M for the variant (Table S2).

**Limited Proteolysis of Recombinant Wild Type and Variant TTR.** Proteolysis at very low enzyme:substrate ratio is a powerful and highly discriminating approach to compare the most flexible and solvent exposed sites, and thus monitor focal stability in the surface topology of native globular proteins. It revealed a surprisingly dramatic difference between wild type and Ser52Pro variant TTR, the former being completely resistant to cleavage even after long incubation or increased protease concentration, whereas the latter was rapidly proteolyzed. Fig. 2*A* shows the electrophoretic pattern of the product of trypsin digestion. After 1 h of incubation the variant TTR released three main polypeptides which we identified by MALDI-MS analysis of the corresponding electro-eluted bands as peptides 16-127 (purple), 49-127 (green) and 81-127 (red) respectively (Fig. 2). In the same lane of the gel the band of the undigested monomer of Ser52Pro TTR was also present (Fig. 2*A*).

Consistent with the protease resistance of wild type TTR, and in sharp contrast to the exquisite sensitivity of the Ser52Pro variant, none of the other recombinant amyloidogenic TTR variant proteins which we tested, Val30Met, Leu55Pro and Val122Ile, were cleaved at all under the conditions used (Fig. S4). In this experiment we monitored the proteolytic cleavage in the early phase of incubation up to 2 h thus revealing that the peptide 49-127 (green box, Fig. S4) is already formed at 3 min of trypsin exposure. The peptide 81-127 (red box, Fig. S4) is most likely a later product derived from a secondary proteolytic cleavage, as are other minor unidentified lower molecular weight fragments.

**TTR Cleavage and Fibril Formation.** Like wild type TTR and all other amyloidogenic TTR variants previously tested, the full length Ser52Pro variant did not form amyloid fibrils in vitro when stirred in solution at physiological pH and ionic strength (Fig. 3*A*). In contrast, when

trypsin was added to the native Ser52Pro TTR solution in PBS at 37°C whilst being stirred at 900 rpm, ThT fluorescence very rapidly increased (Fig. 3*A*). Fibrillogenesis of this variant under physiological conditions was strictly dependent on both proteolytic cleavage and stirring, and the main component of this fibrillar and insoluble material was the same residue 49-127 fragment (Fig. 3*B*, lane c) identified in the natural fibrils (Fig. 3*B*, lane d). The fibrils formed by residue 49-127 variant TTR peptide in vitro showed the pathognomonic amyloid green birefringence under polarized light after staining with Congo red. Transmission electron microscopy showed that the aggregated TTR was almost entirely fibrillar with minimal amorphous material (Fig. 3*C*) which represents much more efficient fibrillar conversion than previously reported for in vitro TTR aggregation (15). Atomic force microscopy (Fig. 3*D*) confirmed the fibrillar ultrastructure. The diffraction pattern obtained from partially aligned Ser52Pro TTR variant amyloid fibrils showed diffraction signals at 4.7 Å and 9.5 Å (Fig. 3*E*), consistent with the cross-β structure previously reported for many different types of amyloid fibrils including Val30Met TTR (16). Although the fibrils were difficult to orient, probably due to their tangled nature (Fig. 3*C*), the diffraction pattern shows increased intensity on the vertical axis compared to horizontal axes supporting the cross-β arrangement whereby β-strands are hydrogen bonded along the length of the fibril with a regular 4.7 Å distance between them. The side chains are accommodated between the β-sheets that are associated with a distance of around 9.5 Å. In addition to the cross-β signals, a strong reflection at 18 Å was observed on the equator of the pattern and this may arise from association of protofilaments within the fibrils.

Despite the intensely fibrillogenic nature of the residue 49-127 fragment of Ser52Pro TTR, addition of the fibrils formed by this polypeptide did not seed amyloid fibril formation by either native intact Ser52Pro TTR or wild type TTR in physiological buffer (Fig. S5).

**3D Crystal Structures.** Both wild type and Ser52Pro TTR crystallized in the commonly reported orthorhombic crystal form (space group $P2_12_12$) that contains a dimer of TTR subunits in the asymmetric unit. The structures are very similar and backbone atoms for 221 residues where the electron density is good, superposed with an RMSD of 0.42 Å. The regions showing the largest differences are displayed in Fig. 4*A*. The region 19-23 of molecule A may be of particular note as a hydrogen bond between Ala19 CO and Tyr114 NH of a symmetry related subunit is a contributor to the limited bonding that stabilizes the tetramer. The positions of Ala19 CO differ by more than 1.1 Å between the two structures suggesting some disturbance of the tetramer but the hydrogen bond with Tyr114 is sustained. The proline substitution was readily modeled into the electron density for the β-turn at position 52 (Fig. 4*B*). However, crucially, the hydrogen bonding network involving Ser52, Glu54 and Ser50 in both TTR subunits in the wild type structure, and including a water molecule in subunit A, is modified in the variant. In the absence of Ser52, its hydrogen bonding partner, the Glu54 carboxylate rotates by 90° and makes new interactions with Lys15 or His56 and no interaction can exist between Pro52 and the Ser50 side chain. Only three hydrogen bonds less than or equal to 3 Å in length remain in the turn of the variant protein (Ser50 CO and Gly53 NH, Ser50 NH and Glu54 CO, Ser50 OG and Glu54 CO) compared to five in wild type TTR. The loss of two hydrogen bonds would be expected to substantially destabilize the turn and the associated C and D strands. Displacement of this loop region has been proposed as the final common pathway for fibrillogenesis in a selection of amyloidogenic TTR variants by exposure of edge strands of the core β-structure of the protein (17). Such movements would certainly increase the accessibility of Lys48 to proteolytic cleavage.

The mechanism of the observed tetramer destabilisation cannot be determined directly from the crystal structure presented but, it is not unreasonable to suppose that the observed loop I and II changes in the crystal structure of Ser52Pro TTR, situated at or close to subunit interfaces, may be vestiges of a conformer population in solution where more extreme structural fluctuations exist. Transient exposure of isolated subunits as occurs in subunit exchange (18) could provide a context in which the lack of subunit stabilising forces of the tetramer allow full expression of the destabilising influence of the Pro52 substitution. For the Ser52Pro variant the cleavage of the 48-49 peptide bond should not result in the dissociation of the 1-48 peptide since many of the bonding interactions remain in place. It is of note, however, that the NH of the 48-49 peptide bond hydrogen bonds to Val28 CO of strand B close to turn I and, while this might be sustained by the new N-terminal generated by cleavage, the separation of this from the new carboxylate of Lys48 must widen from 1.2 to at least 2.8 Å and promote displacement of the CD turn. Departure of the 1-48 peptide caused by shear forces in solution would remove important dimer-dimer interaction regions (19-23) and promote dissociation of the remaining 49-127 fragment.

**Proteolysis of Ser52Pro TTR with Bound Ligands.** Binding of tafamidis and mds84 (13, 14), which both enter the TTR inner channel, had no significant effect on the products (Fig. 5*A*) or kinetics (Fig. 5*B*) of trypsin digestion of Ser52Pro variant TTR. Epigallocatechin, which binds to the outer molecular surface, similarly did not reduce the susceptibility of Ser52Pro TTR to proteolytic cleavage, although appearance of TTR oligomers prevented precise quantification of full length TTR as previously reported (19). Evidently these various, avidly bound ligands do not protect the susceptible TTR sequences despite their potent stabilization of the native tetrameric assembly. Finally we have tested the effect of the two natural ligands of TTR,

thyroxine and retinol binding protein (RBP, Fig. S6), on proteolysis of Ser52Pro TTR and its fibrillogenesis (Fig. 6). Neither of the two interactors protected against the selective cleavage (Inset of Fig. 6) and binding of RBP, but not thyroxine, totally inhibited fibrillogenesis. Our preliminary mass spectrometry analysis suggests that this reflects the capacity of RBP to retain the cleaved monomer within a stabilized native tetramer.

## Discussion

The Ser52Pro TTR variant causes devastating rapidly progressive hereditary neuropathic systemic amyloidosis with extensive visceral and cardiac involvement which is universally fatal in early to mid adult life. Our present characterization of the structure and properties of the Ser52Pro variant provide a compelling biophysical explanation of this aggressive pathology.

The Ser52Pro substitution both destabilizes the native tetramer assembly and makes the protein highly susceptible to a selective, specific proteolytic cleavage at residue 48 to release the *C*-terminal residue 49-127 fragment which is potently amyloid fibrillogenic. The 3D structure of the variant TTR shows no gross structural changes affecting the accessibility of Lys48 that would enhance sensitivity to proteases. The structural similarity with the normal wild type counterpart protein (4) explains the failure of intracellular quality control mechanisms to censor secretion of these pathogenic proteins. However despite the marked overall structural conservation (Fig. 4*A*), a modest difference was observed here in the 3D structure of Ser52Pro TTR (Fig. 4*B*) which is likely to be responsible for its crucial sensitivity to proteolytic cleavage.

The variant Pro52 residue is located in the type 1 β turn that connects β strands C and D, and the dihedral angles of the wild type Ser52 residue enable substitution by proline without adjustment of the main chain path. However the Ser52 side chain participates in a hydrogen

bonding network across the turn in the wild type protein. Loss of this network caused by the proline substitution almost certainly destabilizes the turn and perturbs the adjacent strands, increasing their flexibility, abrogating the protection against proteolysis in the wild type protein, and contributing to the significant observed thermodynamic destabilization.

Exposure of the native Ser52Pro variant TTR tetramer to very low dose trypsin under physiological conditions rapidly generated the same residue 49-127 fragment which is found in ex vivo TTR amyloid fibrils, specifically those designated as type A which are present in patients with other amyloidogenic TTR variants and patients with senile systemic amyloidosis caused by deposition of wild type TTR (20). However, neither wild type TTR nor the other TTR variants we tested, Val30Met, Leu55Pro and Val122Ile, were similarly cleaved in vitro and they are thus notably more stable to proteolysis. Nevertheless it is plausible that in in vivo conditions, in particular shear flow and exposure to hydrophobic surfaces in the dynamic environment of the interstitial space, may promote local structural destabilization (21, 22) and enable proteolytic cleavage. Indeed focal mechanical destabilization of the polypeptide chain is a well known mechanism for priming limited physiological proteolytic cleavage in the homeostasis of haemostatic proteins. The classical example of this mechano-enzymatic mechanism involves the multimeric von Willebrand factor in which shear forces induce a local destabilization and permit the proteolytic cleavage by a specific metalloprotease (23).

Our identification, in the amyloid fibrils in the present propositus, of full length TTR monomers from both the wild type and variant proteins but the highly fibrillogenic residue 49-127 fragment from only the variant, strongly suggests that the native tetrameric TTR variant is the substrate for proteolytic cleavage in vivo rather than already formed fibrils. Furthermore our newly established in vitro method of generating genuine TTR amyloid fibrils after enzymatic

cleavage suggests that proteolysis may be a pre-fibrillar event, at least for this variant, as massive rapid amyloid fibril formation proceeds as soon as the *N*-terminal 48 residue peptide is released. In contrast the recombinant residue 49-127 fragment produced by Mizuguchi et al. (24) gave a very low yield of amyloid fibrils in vitro. This discrepancy highlights new aspects of the TTR amyloid pathway, suggesting that the type of aggregate is strictly dependent on the structural conformation of the precursor. Our finding that fibril formation is much more efficient when the truncated amyloidogenic precursor is cleaved directly from the folded TTR molecule is consistent with the early observation that the intermediate capable of forming amyloid fibrils retains much of the secondary and tertiary structure of native TTR (25).

In conclusion the discovery of the peculiar proteolytic processing of the Ser52Pro variant illuminates a potentially general pathway of TTR amyloidogenesis dictated by the formation of the residue 49-127 polypeptide. It will be interesting, in future, to investigate the possible presence of cleaved TTR or the residue 49-127 fragment in the circulation of patients and carriers of this mutation. Furthermore, since ligands which potently stabilize the native tetrameric assembly of TTR do not protect Ser52Pro TTR against the amyloidogenic cleavage, additional therapeutic approaches to inhibition of TTR amyloidogenesis may be required. It is worth noting that thyroxine, the natural ligand occupying the inner channel of the TTR tetramer, does not prevent either proteolysis or fibril formation. In contrast, RBP, although unable to protect from cleavage, is a very efficient inhibitor of fibrillogenesis. The different effects of thyroxine and RBP on proteolysis and fibrillogenesis are consistent with a sequential two-phase process. The first phase comprises cleavage of the 48-49 peptide bond but does not itself necessarily release the truncated residue 49-127 polypeptide from the intact native tetramer. In the second phase forces, such as those generated by fluid agitation (22), are sufficient to release

the fragments with consequent fibril formation. Thyroxine does not stabilize the tetramer sufficiently to prevent fibrillogenesis, whereas the binding of RBP is adequate to block the second phase, impeding release of the fibrillogenic free fragment.

The discovery and characterization of these crucial new steps in the pathway of TTR amyloid fibrillogenesis could provide novel drug discovery targets as well as offering insight into the mode of action and potential efficacy of current approaches based on drugs occupying the thyroxine binding site.

## Methods

**Limited Proteolysis.** Recombinant wild type, Ser52Pro variant TTR, Val122Ile, Val30Met and Leu55Pro TTR, were individually digested at 1mg/mL in PBS pH 7.4 at 37°C containing trypsin at w/w enzyme:substrate ratios of 1:200. At different times, aliquots of each incubation mixture were stopped by adding PMSF to 1.5 mM, immediately boiled in SDS sample buffer and stored at -20°C before SDS 15% PAGE carried out under reducing conditions. For proteomic characterization of the proteolytic fragments, Coomassie Blue stained bands were electro-eluted, lyophilized, dissolved in 0.2% TFA, mixed with $\alpha$-cyano-4-hydroxycinammic acid (5 mg/mL in acetonitrile, 0.2% trifluoroacetic acid 7:3 v/v), and left to air dry in a metallic sample plate before linear MS analysis (Waters Micromass spectrometer). Horse heart myoglobin was used for mass calibration.

The effect of trypsin was also tested at 1:200 w/w enzyme:substrate ratio in the presence of 5 fold molar excess of tafamidis (14), mds84 (13), and epigallocatechin (19) respectively.

**Amyloid Fibrillogenesis.** Samples of recombinant wild type and Ser52Pro TTR, 100 $\mu$L at 1 mg/mL in PBS pH 7.4 containing 10 µM thioflavin T (ThT) (26), were incubated at 37°C in Costar 96 well blackwall plates sealed with clear sealing film, subjected to 900 rpm double orbital shaking. Bottom fluorescence was recorded at 5 min intervals (BMG LABTECH FLUOstar Omega). After 1 h 5 ng/$\mu$L of trypsin (Promega Trypsin Gold Mass Spectrometry Grade), or buffer alone was added, and fluorescence was

monitored in 3 or more replicate test and control wells for the next 4 h. The data were normalized to the signal plateau at ~ 4 h after the initiation of each reaction. Sample processing for microscopy analyses, and fibrillogenesis assay in the presence of seeds, thyroxine or holo-RBP are described in *SI Methods*.

**Other Methods.** Histology, isolation and chemical characterization of ex vivo amyloid fibrils, DNA sequencing, recombinant TTR production, thyroxine displacement assay, equilibrium denaturation, electron microscopy, atomic force microscopy and X-ray fiber diffraction, X-ray crystal structure determination, native mass spectrometry analysis of the TTR:RBP complex are described in *SI Methods*.

**ACKNOWLEDGMENTS.** The study was supported by the UK Medical Research Council (MR/K000187/1 to V.B.); the UCL Amyloidosis Research Fund and UCL Wolfson Drug Discovery Unit Funds; the Italian Ministry of University and Research (Project FIRB RBFR109EOS to S.G.); Regione Lombardia (V.B.). Core support for the Wolfson Drug Discovery Unit is provided by the UK National Institute for Health Research Biomedical Research Centre and Unit Funding Scheme. The views expressed are those of the authors and not necessarily those of the UK NHS, the UK National Institute for Health Research or the UK Department of Health. We thank Amanda Penco for her assistance with Atomic Force Microscopy measurements and Beth Jones for processing the manuscript.

**Author contributions:** V.B. designed research; P.P.M., R.P., P.P., M.M., M.P., S.G., L.M., S.R., L.C.S., W.C., A.R., J.M., I.C., G.A.T. performed research; P.P.M., R.P., J.D.G., P.P., M.M., S.G., L.M., S.R., L.C.S., W.C., A.R., J.M., I.C., G.W.T., C.V.R., P.N.H., M.S., S.P.W., M.B.P. and V.B. analyzed data. V.B., P.P.M., P.N.H. and M.B.P. wrote the paper which was reviewed and approved by all co-authors.

**Conflict of interest statement:** The authors declare that no conflict of interest exists.

## References


1. Pepys MB (2006) Amyloidosis. *Annu Rev Med* 57(1):223-241.
2. Merlini G, Bellotti V (2003) Molecular mechanisms of amyloidosis. *N Engl J Med* 349(6):583-596.
3. Valleix S, et al. (2012) Hereditary systemic amyloidosis due to Asp76Asn variant $\beta_2$-microglobulin. *N Engl J Med* 366(24):2276-2283.
4. Palaninathan SK (2012) Nearly 200 X-ray crystal structures of transthyretin: what do they tell us about this protein and the design of drugs for TTR amyloidoses? *Curr Med Chem* 19(15):2324-2342.
5. Hammarstrom P, Wiseman RL, Powers ET, Kelly JW (2003) Prevention of transthyretin amyloid disease by changing protein misfolding energetics. *Science* 299(5607):713-716.
6. Westermark P, Sletten K, Johnson KH (1996) Ageing and amyloid fibrillogenesis: lessons from apolipoprotein AI, transthyretin and islet amyloid polypeptide. *Ciba Found Symp* 199:205-218.
7. Thylen C, et al. (1993) Modifications of transthyretin in amyloid fibrils: analysis of amyloid from homozygous and heterozygous individuals with the Met30 mutation. *EMBO J* 12(2):743-748.
8. Bergstrom J, et al. (2005) Amyloid deposits in transthyretin-derived amyloidosis: cleaved transthyretin is associated with distinct amyloid morphology. *J Pathol* 206(2):224-232.
9. Ihse E, et al. (2013) Amyloid fibrils containing fragmented ATTR may be the standard fibril composition in ATTR amyloidosis. *Amyloid* 20(3):142-150.
10. Ihse E, et al. (2008) Amyloid fibril composition is related to the phenotype of hereditary transthyretin V30M amyloidosis. *J Pathol* 216(2):253-261.
11. Gustafsson S, et al. (2012) Amyloid fibril composition as a predictor of development of cardiomyopathy after liver transplantation for hereditary transthyretin amyloidosis. *Transplantation* 93(10):1017-1023.
12. Hawkins PN, Lavender JP, Pepys MB (1990) Evaluation of systemic amyloidosis by scintigraphy with 123I-labeled serum amyloid P component. *N Engl J Med* 323(8):508-513.
13. Kolstoe SE, et al. (2010). Trapping of palindromic ligands within native transthyretin prevents amyloid formation. *Proc Natl Acad Sci USA* 107(47):20483-20488.

14. Bulawa CE, et al. (2012) Tafamidis, a potent and selective transthyretin kinetic stabilizer that inhibits the amyloid cascade. *Proc Natl Acad Sci USA* 109(24):9629-9634.

15. Jiang X, et al. (2001) An engineered transthyretin monomer that is nonamyloidogenic, unless it is partially denatured. *Biochemistry* 40(38):11442-11452.

16. Blake CCF, Serpell LC (1996) Synchrotron X-ray studies suggest that the core of the transthyretin amyloid fibril is a continuous β-helix. *Structure* 4(8):989-998.

17. Serpell LC, Blake CCF (1994) in Amyloid and Amyloidosis 1993, eds Kisilevsky R, Benson MD, Frangione B, Gauldie J, Muckle TJ, Young ID (Pearl River, NY: Parthenon Publishing), pp 447-449.

18. Schneider F, Hammarstrom P, Kelly JW (2001) Transthyretin slowly exchanges subunits under physiological conditions: A convenient chromatographic method to study subunit exchange in oligomeric proteins. *Protein Sci* 10(8):1606-1613.

19. Miyata M, et al. (2010) The crystal structure of the green tea polyphenol (-)-epigallocatechin gallate-transthyretin complex reveals a novel binding site distinct from the thyroxine binding site. *Biochemistry* 49(29):6104-6114.

20. Gustavsson A, et al. (1995) Amyloid fibril composition and transthyretin gene structure in senile systemic amyloidosis. *Lab Invest* 73(5):703-708.

21. Bekard IB, Asimakis P, Bertolini J, Dunstan DE (2011) The effect of shear flow on protein structure and function. *Biopolymers* 95(11):733-745.

22. Mangione PP, et al. (2013) Structure, folding dynamics and amyloidogenesis of Asp76Asn $\beta_2$-microglobulin: roles of shear flow, hydrophobic surfaces and α-crystallin. *J Biol Chem* 288(43):30917-30930.

23. Zhang X, Halvorsen K, Zhang CZ, Wong WP, Springer TA (2009) Mechanoenzymatic cleavage of the ultralarge vascular protein von Willebrand factor. *Science* 324(5932):1330-1334.

24. Mizuguchi M, et al. (2008) Unfolding and aggregation of transthyretin by the truncation of 50 *N*-terminal amino acids. *Proteins* 72(1):261-269.

25. Colon W, Kelly JW (1992) Partial denaturation of transthyretin is sufficient for amyloid fibril formation in vitro. *Biochemistry* 31(36):8654-8660.

26. Naiki H, Higuchi K, Hosokawa M, Takeda T (1989) Fluorometric determination of amyloid fibrils in vitro using the fluorescent dye, thioflavin T1. *Anal Biochem* 177(2):244-249.

27. McNicholas S, Potterton E, Wilson KS, Noble ME (2011) Presenting your structures: the CCP4mg molecular-graphics software. *Acta Crystallogr D Biol Crystallogr* 67(Pt 4):386-394.

28. DeLano WL (2002) in *The PyMOL Molecular Graphics System*, eds DeLano Scientific LLC (San Carlos, CA, USA) http://www.pymol.org

## Figure Legends

**Fig. 1** Ex vivo amyloid fibrils. (*A*) Transmission electron microscopy of amyloid fibrils extracted from spleen (230,000x direct magnification; scale bar, 100 nm). (*B*) SDS 15% PAGE under reducing conditions. Lane a, marker proteins (14.4, 20.1, 30.0, 45.0, 66.0 and 97.0 kDa respectively); lane b, 0.5 μg recombinant Ser52Pro TTR; lane c, 60 μg ex vivo amyloid fibrils from spleen. 1 and 2, bands subjected to mass mapping analysis. (*C*) Tryptic peptides obtained by digestion of SDS-PAGE bands were analyzed by MALDI-MS and nano-LC MS-MS. $MH^+$ monoisotopic values are reported for each peptide with the asterisk indicating the presence of the Ser52Pro substitution. Cysteine is carbamidomethylated.

**Fig. 2.** Limited trypsin proteolysis of wild type and Ser52Pro TTR. (*A*) SDS (15%) PAGE under reducing conditions of wild type and Ser52Pro TTR after incubation at 37°C with trypsin at 1:200 enzyme:substrate ratio for times shown. Wild type TTR alone (a) or with trypsin (b), Ser52Pro TTR alone (c) or with trypsin (d). The three main polypeptides released from Ser52Pro TTR after 1 h of digestion are highlighted with purple, green and red boxes. (*B*) MALDI-MS spectra of the fragments electro-eluted from the bands shown in (*A*) and acquired in linear mode.

**Fig. 3.** Fibrillogenesis of Ser52Pro TTR triggered by release of the residue 49-127 fragment. (*A*) Normalized ThT fluorescence emission from wild type TTR (black) and Ser52Pro TTR (red) fibrillogenesis in the presence (full lines) and absence (dotted lines) of trypsin 5 ng/μL. (*B*) SDS 15% PAGE under reducing conditions. Lane a, marker proteins (14.4, 20.1, 30.0, 45.0, 66.0 and 97.0 kDa); lane b, recombinant Ser52Pro TTR; lane c, in vitro Ser52Pro fibrils; lane d, ex vivo amyloid fibrils from spleen. (*C*) Negatively stained transmission electron micrograph of Ser52Pro TTR amyloid fibrils generated in presence of trypsin and shaking (175,000x direct magnification, scale bar 100 nm). (*D*) Tapping mode AFM image (height data) of Ser52Pro TTR fibrils obtained as in (*A*). Scan size 2.0 μm, Z range 10 nm. (*E*) The X-ray fibre diffraction pattern collected from partially aligned amyloid fibrils formed by Ser52Pro TTR ($\lambda$ = 1.5417 Å, sample to detector distance = 100 nm, exposure

time = 30 s) shows a reflection that is stronger on the meridian at 4.7 Å. A reflection is also highlighted at 9.5 Å and a well oriented signal at 18 Å.

**Fig. 4.** 3D structure of wild type and Ser52Pro TTR. (*A*) Crystal structures of wild type and Ser52Pro TTR were superposed by secondary structure matching (grey-interpreted and presented by CCP4MG (27) and show the close similarity of the folds, RMSD = 0.42Å over 221 residues. Regions of greatest difference are highlighted in blue (Ser52Pro) and magenta (wild type). The CD loops for one subunit of both proteins are shown in green. (*B*) Stick diagram of the CD loop region (carbon-green, oxygen-red, nitrogen-blue) for wild type (left) and Ser52Pro (right) TTR showing the diminished hydrogen bonding network in the vicinity of the proline substitution that may contribute to the enhanced susceptibility of the variant to proteolytic cleavage at Lys48 (28). X-ray data statistics are reported in Table S3.

**Fig. 5.** Limited proteolysis of Ser52Pro TTR with bound ligands**.** (*A*) SDS 15% PAGE under reducing conditions of Ser52Pro TTR alone in presence of DMSO (a) or 5 fold molar excess of epigallocatechin (b), mds84 (c) or tafamidis (d) after incubation at 37°C with trypsin at 1:200 enzyme:substrate ratio for times shown. Marker proteins (14.4, 20.1, 30.0, 45.0, 66.0 and 97.0 kDa) and the non treated Ser52Pro TTR (pre-trypsin) are in the first two lanes respectively. (*B*) Kinetics of proteolytic cleavage of *holo* Ser52Pro TTR in presence of DMSO (black), mds84 (green) or tafamidis (red) monitored by density with time of the intact monomeric TTR band (arrow in panel *A*).

**Fig. 6. Effect of natural interactors, thyroxine and RBP, on proteolysis/fibrillogenesis by Ser52Pro TTR.** Normalized ThT fluorescence emission for trypsin dependent fibrillogenesis of Ser52Pro TTR alone (a) or in presence of 2 fold excess of thyroxine (b), two fold excess of RBP (c) or RBP alone (d). Inset, SDS 15% PAGE under reducing conditions of fibrillogenesis samples before and after 4 h of trypsin digestion. Marker proteins (14.4, 20.1, 30.0, 45.0, 66.0 and 97.0 kDa) are included.

Figure 1

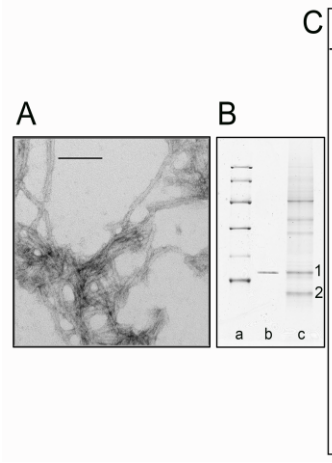


C

| Position | Sequence | MH⁺ (band 1) | MH⁺ (band 2) |
|---|---|---|---|
| **1-15** | GPTGTGESKCPLMVK | 1561.87 | – |
| **16-21** | VLDAVR | 672.40 | – |
| **22-34** | GSPAINVAVHVFR | 1366.77 | – |
| **22-35** | GSPAINVAVHVFRK | 1494.86 | – |
| **35-48** | KAADDTWEPFASGK | 1522.73 | – |
| **36-48** | AADDTWEPFASGK | 1394.63 | – |
| **49-70** | TSESGELHGLTTEEEFVEGIYK | 2455.23 | – |
| **49-70*** | TSEPGELHGLTTEEEFVEGIYK | 2465.22 | 2465.22 |
| **49-76** | TSESGELHGLTTEEEFVEGIYKVEIDTK | 3140.54 | – |
| **49-76*** | TSEPGELHGLTTEEEFVEGIYKVEIDTK | 3150.57 | 3150.58 |
| **77-80** | SYWK | 583.28 | – |
| **81-103** | ALGISPFHEHAEVVFTANDSGPR | 2451.23 | 2451.25 |
| **81-104** | ALGISPFHEHAEVVFTANDSGPRR | 2607.33 | 2607.35 |
| **104-127** | RYTIAALLSPYSYSTTAVVTNPKE | 2645.41 | 2645.43 |
| **105-127** | YTIAALLSPYSYSTTAVVTNPKE | 2489.30 | 2489.33 |

Figure 2

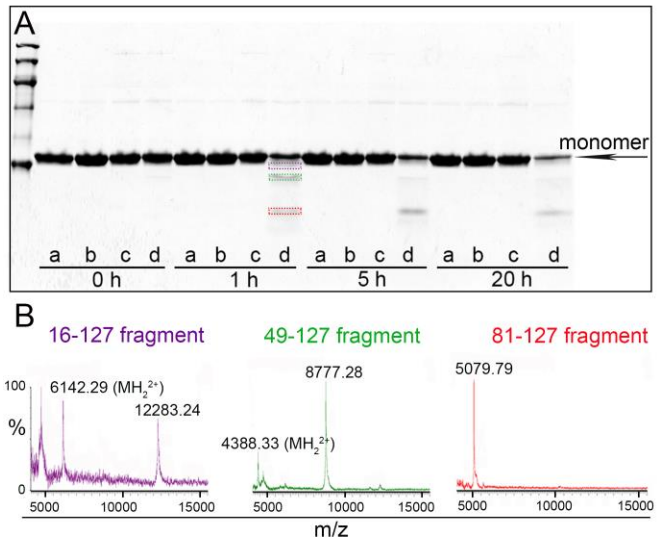
A
monomer
a b c d a b c d a b c d a b c d
0 h
1 h
5 h
20 h
B
16-127 fragment
49-127 fragment
81-127 fragment
6142.29 (MH2 2+)
12283.24
8777.28
4388.33 (MH2 2+)
5079.79
100
%
0
5000
10000
15000
m/z

Figure 3

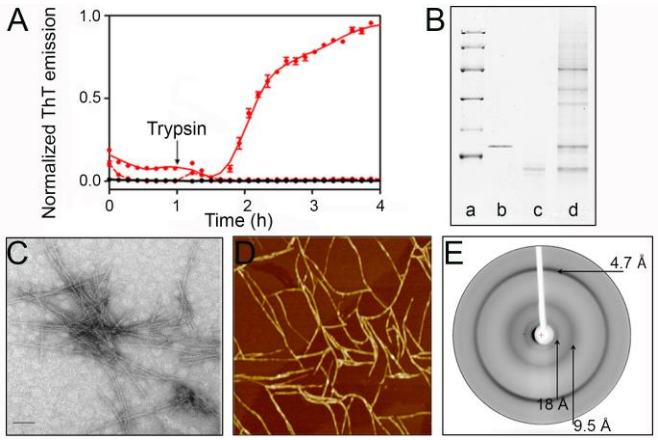
A
Normalized ThT emission
1.0
0.5
0.0
Trypsin
0
1
2
3
4
Time (h)
B
a
b
c
d
C
D
E
4.7 Å
18 Å
9.5 Å

Figure 4

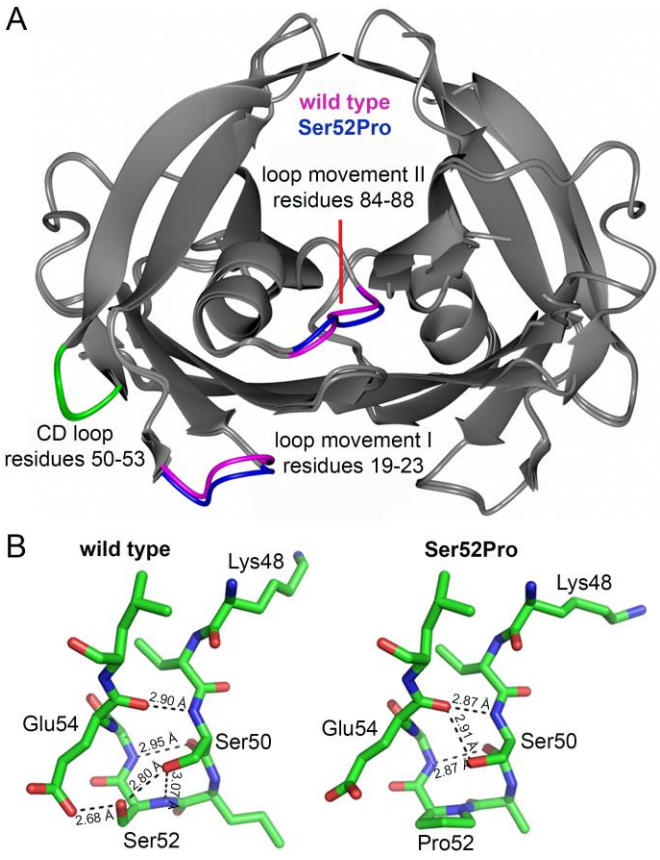
A
wild type
Ser52Pro
loop movement II
residues 84-88
CD loop
residues 50-53
loop movement I
residues 19-23
B
wild type
Lys48
Glu54
Ser50
Ser52
2.90 Å
2.95 Å
2.80 Å
3.07 Å
2.68 Å
Ser52Pro
Lys48
Glu54
Ser50
Pro52
2.87 Å
2.91 Å
2.87 Å

Figure 5

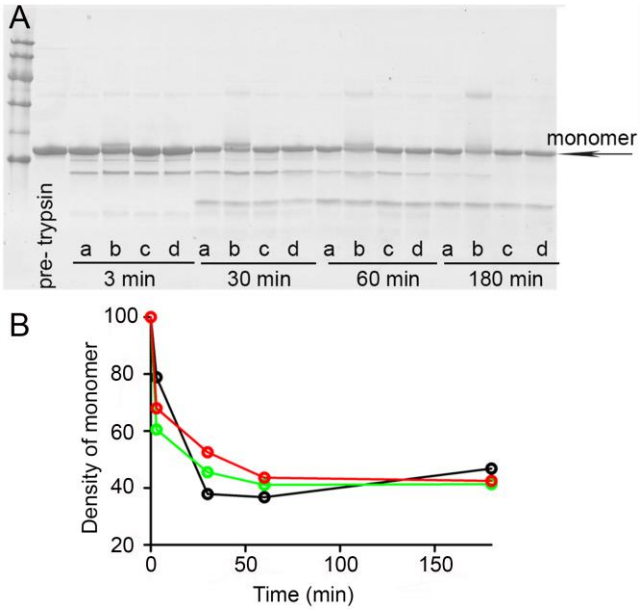
A
monomer
pre- trypsin
a b c d a b c d a b c d a b c d
3 min
30 min
60 min
180 min
B
Density of monomer
100
80
60
40
20
0
50
100
150
Time (min)

Figure 6

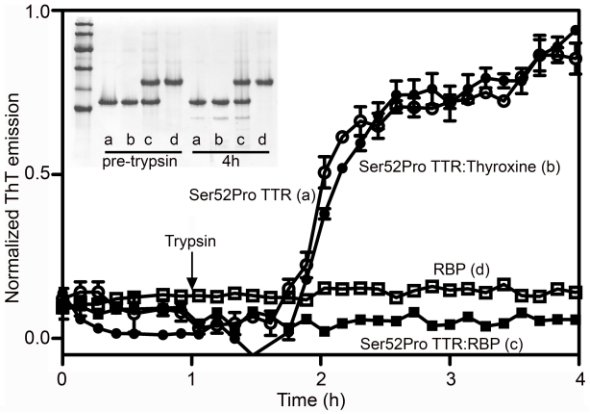
1.0
0.5
0.0
Normalized ThT emission
0
1
2
3
4
Time (h)
a b c d
pre-trypsin
a b c d
4h
Ser52Pro TTR (a)
Ser52Pro TTR:Thyroxine (b)
Trypsin
RBP (d)
Ser52Pro TTR:RBP (c)

SUPPORTING INFORMATION FOR:

# Proteolytic cleavage of Ser52Pro variant transthyretin triggers its amyloid fibrillogenesis

P. Patrizia Mangione, Riccardo Porcari, Julian D. Gillmore, Piero Pucci, Maria Monti, Mattia Porcari, Sofia Giorgetti, Loredana Marchese, Sara Raimondi, Louise C. Serpell, Wenjie Chen, Annalisa Relini, Julien Marcoux, Innes Clatworthy, Graham W. Taylor, Glenys A. Tennent, Carol V. Robinson, Philip N. Hawkins, Monica Stoppini, Stephen P. Wood, Mark B. Pepys, and Vittorio Bellotti

# TABLE OF CONTENTS

*Page*

## SI Methods

**Patients.** The study was carried out in accordance with the Declaration of Helsinki and was approved by the Royal Free Hospital Ethics Committee. All patients provided informed written consent.

**Histology.** Amyloid deposits were identified in fresh frozen tissue sections by alkaline alcoholic Congo red staining with pathognomonic green birefringence in cross polarized light (1) and fibril types determined by standard immunohistochemical methods.

**Isolation and Chemical Characterization of Ex vivo Amyloid Fibrils.** Amyloid fibrils were isolated from spleen specimens by water extraction after repeated homogenization in 140 mM NaCl, 10 mM Tris, 10 mM EDTA, 0.1% w/v $NaN_3$, 1.5 mM PMSF, pH 8.0. Lyophilized fibrils (60 μg) were separated on SDS 15% PAGE carried out under reduced conditions and, after staining with colloidal Coomassie Blue, excised bands underwent in situ proteolytic digestion (2) before analysis of the extracted peptide mixtures by MALDI-MS (ABI SCIEX 4800 MALDI TOF-TOF mass spectrometer) and by nano LC-MS/MS (Agilent Technologies CHIP MS Ion Trap XCT Ultra with capillary 1100 HPLC system and a chip cube) with raw data analysis by in-house Mascot database searching (Matrix Science, Boston, USA). Unstained fibril samples from the SDS-PAGE were transferred to a PVDF membrane and the same protein bands were analyzed by *N*-terminal sequencing (Applied Biosystems Procise HT49 Protein Sequencer).

**DNA Sequencing.** Genomic DNA was extracted from anticoagulated whole blood, TTR exons amplified by PCR and sequenced.

**Recombinant TTR Production.** Recombinant wild type, Ser52Pro variant TTR and other amyloidogenic TTR variants, Val30Met, Leu55Pro and Val122Ile,were expressed and purified as previously described (3). For Ser52Pro TTR, the Stratagene QuickChange site directed mutagenesis kit was used with the primer sequence GGAAAACCAGTGAG<u>CCT</u>GGAGAGCTGCATG containing the underlined codon for proline at position 52.

**Thyroxine Displacement Assay.** Binding by recombinant Ser52Pro variant TTR was tested by measuring the concentration of competing ligands, mds84 and tafamidis, able to displace 50% of $^{125}$I-thyroxine bound by TTR, as previously described (4).

**Equilibrium Denaturation.** TTR stability at 0.10 mg/mL was studied as a function of Gdn-SCN concentration in 50 mM phosphate, 1 mM EDTA, 1 mM DTT, pH 7.0, at 25°C for 24 h. Denaturation curves were derived from the ratio between tryptophan fluorescence emission intensities at 355 nm (unfolded) and 335 nm (folded) following excitation at 295 nm (Perkin Elmer LS55 spectrofluorimeter) (5).

**Microscopy Analyses.** For electron and atomic force microscopy analyses, PMSF to 1 mM was added to Ser52Pro TTR fibrils, obtained as described in the main text, and the fibrils were then centrifuged at 10,600 g and resuspended twice before dilution 1:10 with water. After two washings, fibrils were also analyzed by SDS 15% PAGE under reducing conditions.

**Electron Microscopy.** Formvar-coated copper EM grids were placed coated side down onto each sample and incubated for 2 min before blotting with filter-paper to remove excess solvent and staining with 2% w/v uranyl acetate for 2 min. After further blotting and drying in air, transmission electron microscope (CM120) images were obtained at 80 keV.

**Atomic Force Microscopy.** A 10 μL aliquot of fibrils was deposited on freshly cleaved mica and dried under mild vacuum. Tapping mode AFM images were acquired in air (Dimension 3000 SPM with "G" scanning head, maximum scan size 100 μm, driven at 320-340 kHz with scan rate 0.5-1.0 Hz by Digital Instruments, Veeco, Nanoscope IIIa controller and Olympus OMCL-AC160TS single beam uncoated silicon cantilevers).

**X-ray Fiber Diffraction.** Ser52Pro TTR fibrils were diluted to approximately 10 mg/mL in filtered MilliQ water and allowed to align between two wax-tipped capillary tubes. The partially aligned sample was mounted on a goniometer head and X-ray diffraction data were obtained with a Rigaku CuKα (λ 1.5419 Å)

rotating anode generator and collected using VariMax-HF mirrors and a Saturn 944+ CCD detector with exposure times of 15-30 s and specimen to detector distance of 50 or 100 mm. Diffraction data were displayed using Mosflm and converted to a TIFF file for inspection in Clearer (6).

**X-ray Crystal Structure Determination.** Orthorhombic protein crystals were grown by hanging drop vapor diffusion at pH 7.4 using PEG400 as the precipitant (7). X-ray diffraction data were collected on beamline I04 and I04-1 at the Diamond Light Source, Oxon, UK; diffraction images were integrated by XDS (8) scaled by SCALA (9), and phases were determined by molecular replacement with PHASER (10) using PDB code 1DVQ as the search model. Protein models were built with COOT (11) and refined with REFMAC (12).

**Cross Seeding Fibrillogenesis.** ThT emission in the 96 well blackwall plate containing wild type and Ser52Pro TTR was monitored in the presence of 0.1 mg/ml Ser52Pro TTR fibrils produced with trypsin and then treated with PMSF. Relative intensities of fluorescence were monitored in 3 replicate test and control wells for the next 7 h.

**Mass Spectrometry Analysis of Native TTR-RBP Complex.** Isolated RBP (Sigma) was incubated with one molar equivalent of retinol to produce holo-RBP. Both this and isolated recombinant Ser52Pro TTR were buffer exchanged into 200 mM ammonium acetate pH 7.4 using Micro Bio-Spin size exclusion chromatography columns (BioRad). Protein concentrations were determined by $A_{280}$ 26,595 and 18,450 $M^{-1}$ $cm^{-1}$ for RBP and TTR respectively. Mixtures of TTR with 2 molar equivalents of holo-RBP were loaded into in-house prepared glass capillaries for nano-electrospray analysis (13) using a Q-TOFII instrument (Micromass), modified for the transmission of large complexes (14). Capillary, cone and transfer voltages were 1.7 kV, 100 V and 10 V respectively, with the backing pressure in the transfer region at 8.8 mbar. Calibration was with caesium iodide at 100 mg/ml and mass spectra were analysed with MassLynx V4.1.

**Amyloid Fibrillogenesis with Natural Ligands**. Amyloid fibrillogenesis was carried out in the presence of 2 fold molar excess of either thyroxine or holo-RBP. Pre-and post-trypsin (4 h) digestion samples were analyzed by SDS 15% PAGE under reducing conditions as above described.

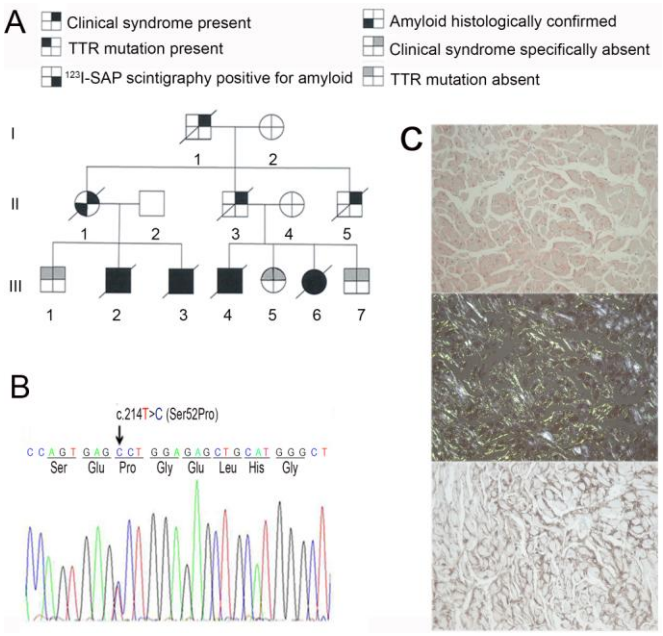


**Fig. S1.** Hereditary Ser52Pro TTR amyloidosis. *(A)* Pedigree of the affected kindred. Squares, males; circles, female; slashes, deceased. *(B)* Partial sequence chromatogram of exon 4 of the transthyretin gene showing the nucleotide substitution identified in affected family members. *(C)* Abundant cardiac amyloid in patient (above, Congo red stain, bright field; centre, Congo red stain, cross polarized light; below, immunohistochemical stain with anti-TTR antibody).

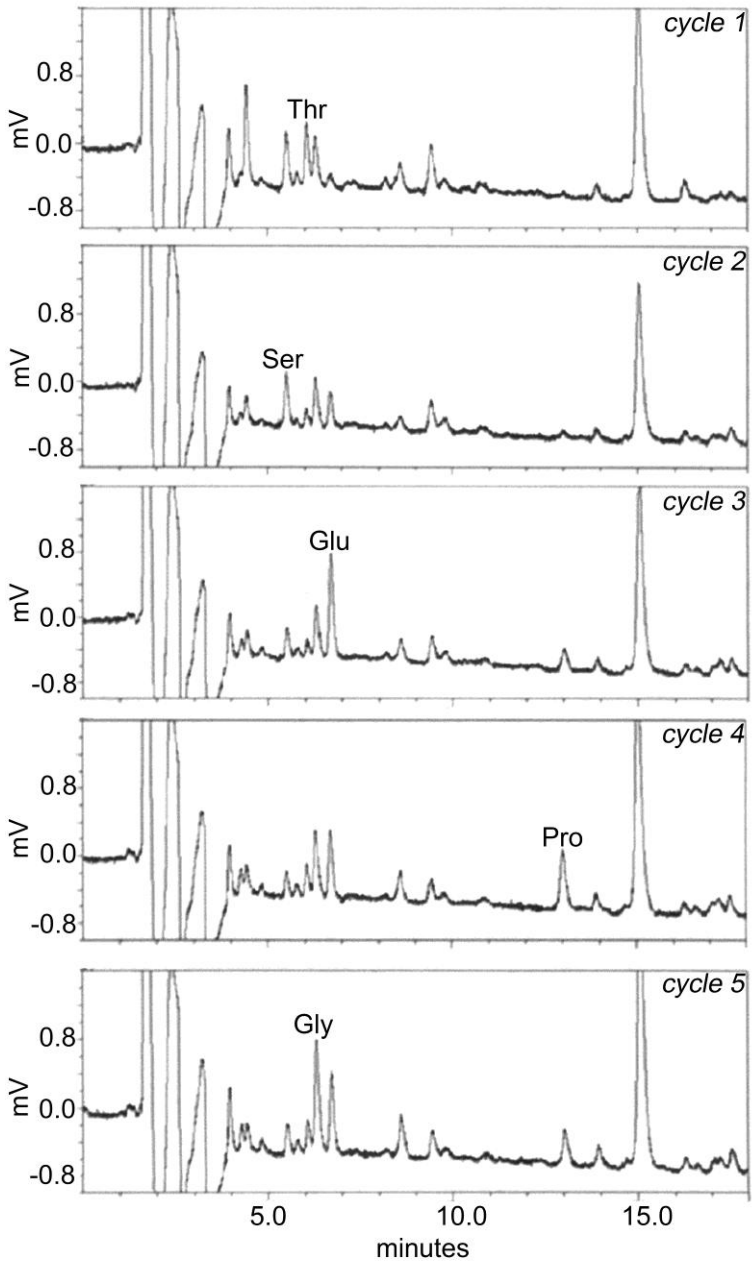


**Fig. S2.** *N*-terminal sequence of TTR fragment from ex vivo amyloid fibrils. Five cycles of Edman *N*-terminal sequencing of band 2 from the PAGE in Fig. 1*B* which had been blotted onto PVDF membrane, yielded the sequence Thr-Ser-Glu-Pro-Gly, corresponding to residues 49-53 of variant TTR with Pro in position 52.

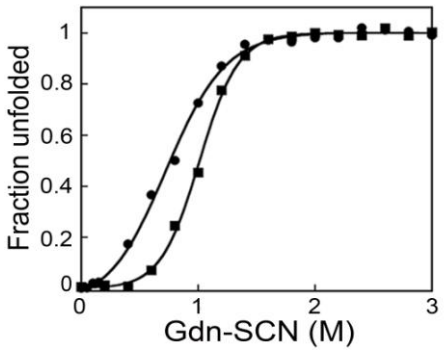


**Fig. S3.** Thermodynamic stability of wild type and Ser52Pro TTR. Gdn-SCN denaturation curves of wild type TTR (squares) and Ser52Pro variant TTR (circles). Experimental data were fitted to a single transition as described (5) and converted to the unfolded fraction using $f_U = (y–y_N)/(y_U–y_N)$, where $y$ is the ratio between 355 nm and 335 nm fluorescence emission intensities at a given denaturant concentration, $y_N$ and $y_U$ are the values of native and unfolded protein, respectively, extrapolated from the pre- and post-transition baselines.

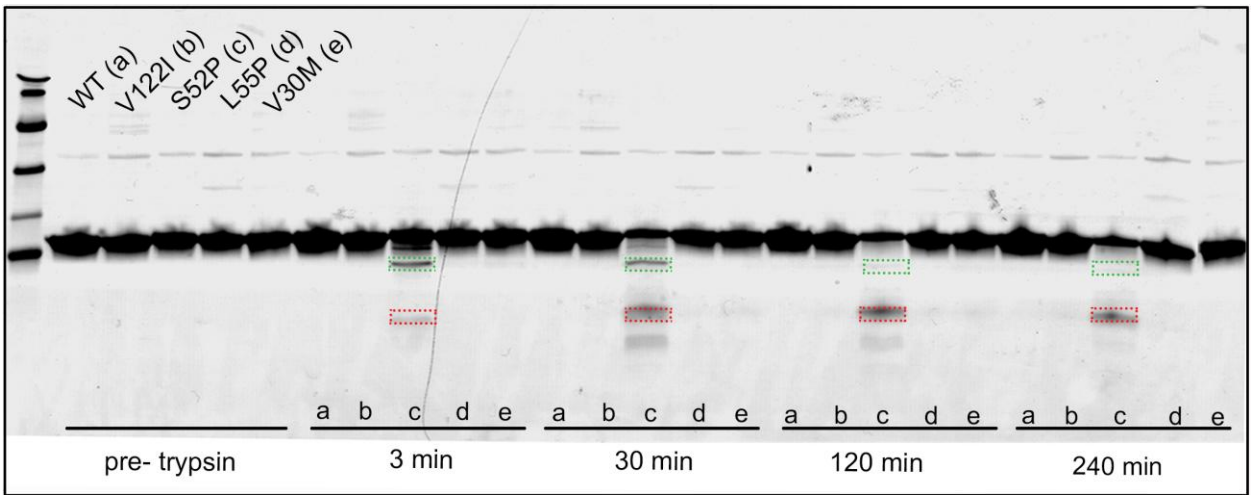


**Fig. S4.** Limited *in vitro* tryptic proteolysis cleaves Ser52Pro but not other TTR isoforms. SDS 15% PAGE under reducing conditions of wild type (a), Val122Ile (b), Ser52Pro (c), Leu55Pro (d) and Val30Met TTR (e) after incubation at 37°C with trypsin at 1:200 enzyme:substrate ratio for times shown. Highlighted in green and red boxes the peptides 49-127 and 81-127 released from Ser52Pro TTR.

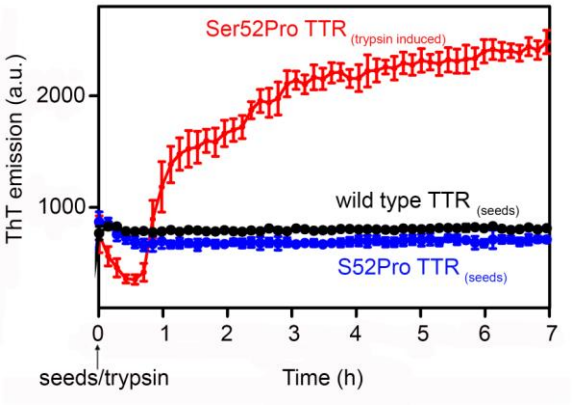


**Fig. S5.** Cross seeding fibrillogenesis experiments. Relative intensities of ThT emission, after subtraction of the pre-trypsin fluorescence, were plotted. Means (SD) of 3 replicates are shown.

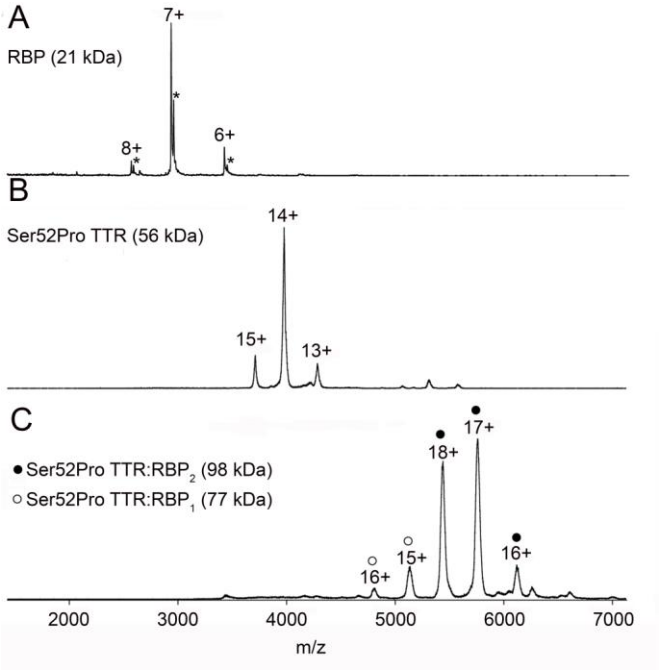


**Fig. S6.** Mass spectrometry of the native Ser52Pro TTR-$RBP_2$ complex. Mass spectra were obtained for (*A*) monomeric RPB; asterisks indicate the presence of retinol bound by RBP. (*B*) tetrameric Ser52Pro TTR and, (*C*) Ser52Pro TTR-$RBP_2$ complex.

## Table S1. Binding of stabilizers by TTR

| | $IC_{50}$ (μM) mean (SD), *n* = 3 | |
|---|---|---|
| **Ligand** | **Wild type TTR** | **Ser52Pro TTR** |
| **mds84** | 0.13 (0.02) | 0.14 (0.02) |
| **tafamidis** | 0.3 (0.04) | 0.3 (0.05) |

Comparative binding capacity of wild type and Ser52Pro variant TTR measured by displacement of the natural ligand, thyroxine, in presence of increasing concentrations of two potent stabilizers (4). $IC_{50}$ values represent the ligand concentration reducing the binding of $^{125}$I-thyroxine by wild type and Ser52Pro variant TTR by 50%.

## Table S2. Thermodynamic parameters of Gdn-SCN induced unfolding

| | $C_m$ (M) | $\Delta G°(H_2O)$ (kcal mol$^{-1}$) | *m* (kcal mol$^{-1}$ M$^{-1}$) |
|---|---|---|---|
| **Wild type TTR** | 1.03 (0.02) | 4.42 (0.25) | 4.31 (0.32) |
| **Ser52Pro TTR** | 0.80 (0.06) | 2.11 (0.50) | 2.58 (0.44) |

The change of fluorescence as a function of denaturant concentration was analyzed as previously reported (15). Values of midpoint denaturant concentration ($C_m$), free energy in absence of denaturant ($\Delta G°(H_2O)$) and dependence of $\Delta G$ on denaturant concentration (*m* value) are mean (SD) of three independent experiments.

**Table S3. Crystallographic statistics**

| Structure | Wild type TTR | Ser52Pro TTR |
|---|---|---|
| **PDB Code** | 4MRB | 4MRC |
| **Beamline** | DLS I04-1 | DLS I04 |
| **Wavelength (Å)** | 0.920 | 0.979 |
| **Space group** | $P2_12_12$ | $P2_12_12$ |
| **Cell dimensions (Å)** | 84.21x41.32x63.01 | 85.41x42.02x63.68 |
| **Resolution (Å)** | 42.10-1.27 | 85.41-1.54 |
| **Completeness %** | 99.7 | 99.7 |
| **Multiplicity** | 12.9 | 4.9 |
| **Total reflections** | 754151 | 170272 |
| **Unique reflections** | 58650 | 34619 |
| **$R_{merge}/R_{pim}(I+/-)$[a]** | 0.057 (0.626) / 0.024 (0.266) | 0.055 (0.573) / 0.019 (0.433) |
| **Reflections used for R-free value** | 2962 | 1742 |
| **RMSD of bond length(Å)/angles (°)** | 0.033/2.79 | 0.019/1.78 |
| **R/R-free value** | 0.166/0.209 | 0.160/0.228 |

[a] values in parenthesis are for the highest resolution shell.

**References**


1. Putchler H, Sweat F, Levine M (1962) Binding of Congo Red by amyloid. *J Histochem Cytochem* 10:355–364.
2. Troise F, et al. (2011) A novel ErbB2 epitope targeted by human antitumor immunoagents. *FEBS J* 278 (7):1156-1166.
3. Lashuel HA, Lai Z, Kelly JW (1998) Characterization of the transthyretin acid denaturation pathways by analytical ultracentrifugation: implications for wild-type, V30M, and L55P amyloid fibril formation. *Biochemistry* 37(51):17851-17864.
4. Kolstoe SE, et al. (2010). Trapping of palindromic ligands within native transthyretin prevents amyloid formation. *Proc Natl Acad Sci USA* 107(47):20483–20488.
5. Hammarstrom P, Wiseman RL, Powers ET, Kelly JW (2003) Prevention of transthyretin amyloid disease by changing protein misfolding energetics. *Science* 299(5607):713–716.
6. Makin OS, Sikorski P, Serpell LC (2007) CLEARER: a new tool for the analysis of X-ray fibre diffraction patterns and diffraction simulation from atomic structural models. *Appl Cryst* 40(5):966-972.
7. Trivella DB, Sairre MI, Foguel D, Lima LM, Polikarpov I (2011) The binding of synthetic triiodo l-thyronine analogs to human transthyretin: molecular basis of cooperative and non-cooperative ligand recognition. *J Struct Biol* 173(2):323-332.
8. Kabsch W (2010) XDS. *Acta Crystallogr D Biol Crystallogr* 66(Pt 2):125-132.
9. Evans P (2006) Scaling and assessment of data quality. *Acta Crystallogr D Biol Crystallogr* 62(Pt 1):72-82.
10. McCoy AJ, et al. (2007) Phaser crystallographic software. *J Appl Crystallogr* 40(Pt 4):658-674.
11. Emsley P, Cowtan K (2004) Coot: model-building tools for molecular graphics. *Acta Crystallogr D Biol Crystallogr* 60(Pt 12 Pt 1):2126-2132.
12. Murshudov GN, et al. (2011) REFMAC5 for the refinement of macromolecular crystal structures. *Acta Crystallogr D Biol Crystallogr* 67(Pt 4):355-367.
13. Hernandez H & Robinson CV (2007) Determining the stoichiometry and interactions of macromolecular assemblies from mass spectrometry. *Nat Protoc* 2(3):715-726.

14. Sobott F, Hernandez H, McCammon MG, Tito MA, & Robinson CV (2002) A tandem mass spectrometer for improved transmission and analysis of large macromolecular assemblies. *Anal Chem* 74(6):1402-1407.

15. Santoro MM, Bolen DW (1988) Unfolding free energy changes determined by the linear extrapolation method. 1. Unfolding of phenylmethanesulfonyl α-chymotrypsin using different denaturants. *Biochemistry* 27(21):8063-8068.